remote sensing

MDPI

Article

Testing the Impact of Pansharpening Using PRISMA Hyperspectral Data: A Case Study Classifying Urban Trees in Naples, Italy

Miriam Perretta [1,2], Gabriele Delogu [3,4], Cassandra Funsten [1], Alessio Patriarca [4], Eros Caputi [3,4] and Lorenzo Boccia [1,2,*]

1 Department of Architecture, University of Naples Federico II, Via Forno Vecchio, 36, 80134 Naples, Italy; miriam.perretta@unina.it (M.P.); cassandracarroll.funsten@unina.it (C.F.)
2 NBFC, National Biodiversity Future Center, 90133 Palermo, Italy
3 Department of Economics, Engineering, Society and Business Organization (DEIM), Tuscia University, Via del Paradiso, 47, 01100 Viterbo, Italy; gabriele.delogu@unitus.it (G.D.); eros.caputi@unitus.it (E.C.)
4 Department of Agricultural and Forestry Sciences (DAFNE), Tuscia University, Via S. Camillo de Lellis, 01100 Viterbo, Italy; alessio.patriarca@unitus.it
* Correspondence: lorenzo.boccia@unina.it; Tel.: +39-0812-539-151

Abstract: Urban trees support vital ecological functions and help with the mitigation of and adaption to climate change. Yet, their monitoring and management require significant public resources. remote sensing could facilitate these tasks. Recent hyperspectral satellite programs such as PRISMA have enabled more advanced remote sensing applications, such as species classification. However, PRISMA data's spatial resolution (30 m) could limit its utility in urban areas. Improving hyperspectral data resolution with pansharpening using the PRISMA coregistered panchromatic band (spatial resolution of 5 m) could solve this problem. This study addresses the need to improve hyperspectral data resolution and tests the pansharpening method by classifying exemplative urban tree species in Naples (Italy) using a convolutional neural network and a ground truths dataset, with the aim of comparing results from the original 30 m data to data refined to a 5 m resolution. An evaluation of accuracy metrics shows that pansharpening improves classification quality in dense urban areas with complex topography. In fact, pansharpened data led to significantly higher accuracy for all the examined species. Specifically, the *Pinus pinea* and *Tilia* x *europaea* classes showed an increase of 10% to 20% in their F1 scores. Pansharpening is seen as a practical solution to enhance PRISMA data usability in urban environments.

Keywords: PRISMA; hyperspectral data; pansharpening; data enhancement; spatial resolution; geospatial analysis; urban tree classification; biodiversity monitoring

Citation: Perretta, M.; Delogu, G.; Funsten, C.; Patriarca, A.; Caputi, E.; Boccia, L. Testing the Impact of Pansharpening Using PRISMA Hyperspectral Data: A Case Study Classifying Urban Trees in Naples, Italy. *Remote Sens.* **2024**, *16*, 3730. https://doi.org/10.3390/rs16193730

Academic Editors: Jaime Zabalza, Yijun Yan and Jinchang Ren

Received: 2 August 2024
Revised: 20 September 2024
Accepted: 2 October 2024
Published: 8 October 2024

1. Introduction

According to the United Nations' 2018 *World Urbanization Prospects Report*, the proportion of the world's population living in urban areas is expected to exceed 68% by 2050 [1], with this figure rising to 86% in developed regions. Consequently, cities must address their social and environmental vulnerabilities regarding the challenges posed by climate change [2–4]. In urban environments, vegetation plays a pivotal role in terms of its ecological functions and its potential as a nature-based solution to the adverse consequences of climate change [2,5–7]. Trees, in particular, perform important services such as improving air quality, reducing runoff and erosion, and lowering surface temperatures [2,8,9]. They also contribute to the aesthetics of the landscape and provide habitats and ecological corridors for a variety of species, increasing connectivity between areas of significant biodiversity [10–12]. Furthermore, trees have been shown to promote social cohesion [13] and economic growth [14]. There is also a growing interest in the carbon storage functions of

urban trees and peri-urban forests [15]. Policy at all levels, from international to local, has come to recognize the importance of urban trees for human and ecosystem wellbeing and makes demands on public administrations to increase, monitor, and manage urban tree cover accordingly [16]. For example, the United Nation's Sustainable Development Goal (SDG) 11.7 [17] and the *New Urban Agenda* [18] both call for increasing equitable access to public green spaces. At a national level, the future fourth Italian National Inventory of Forests and Forest Carbon Pools, planned for 2025, will include an increased focus on urban forests [19]. The National Biodiversity Future Center (NBFC) [20,21], established as part of Italy's post-COVID-19 National Recovery and Resilience Plan (NRRP) [22], is at the forefront of tackling biodiversity loss in Italy, which threatens essential ecosystem services.

However, implementing such policies is no simple feat. In increasingly complex governance systems, it often requires the coordination of very diverse stakeholders, including professionals and department directors working for municipal administrations, employees of private companies receiving public tenders, workers who carry out management tasks as a requirement for receiving public income or as rehabilitation, and non-profit associations, organizations, and citizens that adopt green spaces or volunteer their time for its upkeep [23]. Such a complex sharing of responsibility for urban and peri-urban trees and forests depends on efficient and up-to-date monitoring.

Government agencies can improve their ability to monitor environmental resources and biodiversity conservation by using innovative tools and techniques. Indeed, information on the spatial distribution of tree species and vegetation maps are particularly useful for biodiversity monitoring [24,25]. The availability of land cover information and the classification of urban tree species could be greatly facilitated by remote sensing (RS) with different data sources, such as very high resolution imagery, light detection and ranging (LiDAR) technology, and hyperspectral imagery (HSI) [2,11]. The spatial resolution, radiometric resolution, and temporal resolution of imagery has increased with technological developments along with the availability of a growing number of satellite platforms [26]. Moreover, thanks to spectroscopy satellite missions, such as The Hyperspectral Precursor of the Application Mission (PRISMA) or the Environmental Mapping and Analysis Program (EnMAP) hyperspectral mission, very high spectral resolution has been achieved [27].

PRISMA, launched by the Italian Space Agency (ASI) in 2019, and EnMAP, launched by the German Aerospace Agency in 2022, are both in operational phases [28,29]. Both high spectral resolution imaging spectroscopy missions produce data with a 30 km swath width. PRISMA is a first-generation model to test and advance hyperspectral imaging technology for practical applications [30]. EnMAP is quite similar and is also an experimental satellite [31]. By exploiting a very high spectral resolution, both missions provide additional information compared to multispectral missions, with which synergistic applications are expected [28,31]. Hyperspectral data are widely used for tree classification [32] because they provide more accurate results [33]. In particular, PRISMA data have shown excellent results in spectral separability compared to multispectral data [34]. Other platforms are also expected to become available soon, such as CHIME (Copernicus Hyperspectral Imaging Mission for the Environment), developed by the European Space Agency [27].

Hyperspectral data at a spatial resolution of 30 m $\times$ 30 m are excellent for classifying images in natural environments [34]. However, this spatial resolution is not ideal in urban environments, where images are typically composed of spectrally mixed pixels [35], canopies are fragmented, and are often made up of different species grouped close together [2]. Viable techniques that overcome these limitations and increase the potential of using HIS for urban classification include spectral unmixing and subpixel analysis [35,36]. Recent developments in EO technology have also introduced alternatives that improve the spatial resolution of hyperspectral data using pansharpening, if the panchromatic band is available, or hypersharpening when data are fused with higher spatial resolution data, if available [37,38].

Previous studies [37–39] have explored the potential of hypersharpening by showing that it is appropriate to use multispectral data with a medium resolution satellite, such as

Sentinel 2, for data fusion with hyperspectral data. This technique requires both overlapping acquisition dates, as well as very reliable geocoding and the spatial alignment of the two datasets [39]. Pre-processed products that are easily and directly usable are provided by satellite data distribution agencies. For example, ASI distributes the L2D PRISMA data, an atmospherically corrected and orthorectified reflectance data [30]. Of course, the orthorectification process is an essential step in data fusion involving products from different sensors, especially regarding areas with complex topography. Moreover, despite the convenience of L2D level preprocessing, the PRISMA technical documentation [40] guarantees a planimetric accuracy of no more than 200 m for standard preprocessing without ground control points (GCPs). Thus, fusing data from different satellites in urban areas poses significant challenges related to such factors as the presence of buildings and complex topography. Unless spatial misalignments are carefully addressed to avoid unreliable approximations, these procedures produce outcomes that are not always predictable and may be more complex compared to pansharpening.

In hypersharpening, algorithms must work with a sharpening image that was acquired by a different satellite and consequently shifted in time and taken from a different angle [38,41]. The use of coregistered panchromatic images would avoid these problems. It should be noted that pansharpening only improves the spatial resolution since it only uses the panchromatic band [38]. It is therefore of interest to understand whether the pansharpening techniques often used to improve image interpretation can also be used to improve data classification. One of the objectives of the PRISMA satellite, which is a precursor to the application mission, is to test the feasibility of pansharpening hyperspectral data using a coregistered pan image [30,42], which can provide greater reliability and simplicity of use. This paper aims to respond to this challenge and show a case study example of a practical application.

Specifically, this study's main objectives are:

1. To evaluate the contribution of pansharpening to improving image classification accuracy using hyperspectral data so that it is also useful in an urban setting;
2. To apply the method to a real-world problem, specifically urban tree monitoring, through a simple pansharpening application that only uses the more easily accessible panchromatic band.

To achieve the first objective, results derived using an unrefined PRISMA image with a 30 m ground sampling distance (GSD) are compared to results obtained from classifying an enhanced PRISMA image that has a 5 m spatial resolution achieved through pansharpening. For this comparison, each result is statistically evaluated according to several accuracy metrics and ground truth points (GTPs).

To achieve the second objective, the study classifies the most common tree species in a selected region within the metropolitan city of Naples, Italy. Due to its high settlement density and relatively low amount of urban green spaces, Naples depends on the many services provided by urban trees, and has been carrying out several initiatives over the past few years to improve and manage their urban tree cover. Tree inventories are an important tool in this regard, but take up a significant amount of the public authority's resources, which could be used more efficiently with improved knowledge of trees' spatial distribution.

In order to carry out its objectives, the study is laid out as follows: Section 1 contains the preceding introduction describing relevant background information and identifying research objectives and contributions; Section 2 describes the materials and methods employed, beginning with a brief presentation of the study area, followed by a detailed explanation of the data preparation, the pansharpening method, and the classification procedure, including the related selection of ground truths (GTs) and classes; Section 3 contains the results, presenting the accuracy values obtained with the original image (GSD 30 m) and the enhanced image (GDS 5 m); Section 4 discusses key findings in the context of the literature and concludes with the investigation's main contributions, their implications for research and for practice, their limitations, and some suggestions for future directions.

Finally, this study makes the following contributions:

- It introduces a novel application using pansharpening techniques to improve classification performance by enhancing the spatial resolution of PRISMA hyperspectral data and demonstrates its efficiency with a case study example;
- It demonstrates a practical real-world use of pansharpened image classification for urban tree monitoring, which could help municipalities that are currently struggling to meet international and national policy demands.

2. Materials and Methods

2.1. Study Area

The study area, shown in Figure 1, is an urban area located in the western part of the city of Naples, the regional capital of Campania in southern Italy. This study area presents an interesting opportunity to test out pansharpening in an urban area. Naples shares many struggles in managing urban trees common throughout southern Europe.

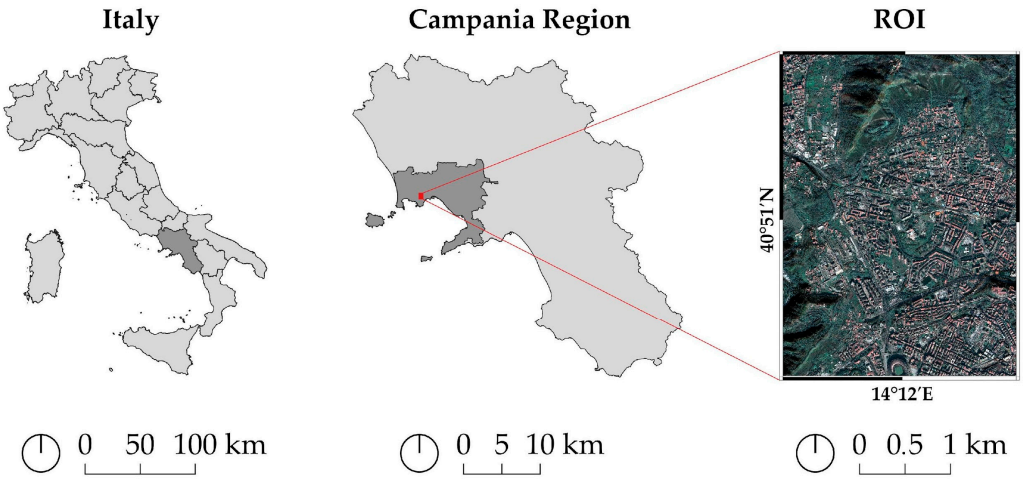

Figure 1. Study area—Region of interest (ROI).

The metropolitan city of Naples has a population of just under 3,000,000 individuals (Istat 2023), and is spread over 1171 km^2 with an extremely high population density of 2519 residents per km^2 [43]. In the European Commission's 2023 *Quality of Life in European Cities Perception Survey*, only 66% of participating residents reported being satisfied with their city, placing Naples 5th from the bottom in an investigation of 83 cities across the European Union (EU), European Free Trade Association (EFTA), the United Kingdom, the western Balkans, and Türkiye (European Commission, 2023). Aside from poor satisfaction with employment, safety, government, healthcare, public transport, and cultural facilities, Naples also stood out as ranking 8th from last for noise (only 38% of participants were satisfied with the noise level), 5th from last for satisfaction with cleanliness (25% satisfied), 6th from last for being a good place for older people to live (only 55% of participants agreed), 4th from last for being a good place for families with young children (only 58% agreed), and 2nd from last for satisfaction with public spaces (45% satisfied). All of these components contributing to quality of life are strongly related to the presence of urban green spaces, which provides opportunities for cohesion, abates noise, and improves city decor, among other benefits. That is why the Sustainable Development Goal (SDG) target 11.7 specifically aims to "provide universal access to safe, inclusive, and accessible green and public spaces, in particular for women and children, older persons, and persons with disabilities" [17]. Most relevantly, Naples scored absolutely last for satisfaction with green spaces in the city (only 31% of residents were satisfied), with the report identifying a strong correlation between accessibility and spatial distribution.

Specifically, as of the city's last Tree Audit in 2021, the municipality of Naples included 5,554,236 m^2 of green spaces, which were challenging to maintain due to diminishing staff, which fell by 77% between 2016 and 2021 [44]. Although the city was responsible

for 50 public parks, only 36 of these were open to the public. However, at the time of the audit, the municipality was active in approving the financing and construction of several renovations and new parks, as well as for other urban greening measures.

In terms of tree cover, the municipality estimated having about 40,000 trees, based on a partial inventory of 28,213 specimens. A total of 9% of these were found to be at high or extreme risk of collapsing. In fact, between 2016 and 2021, 2791 trees had to be removed, mainly due to collapses or damage caused by extreme weather events. During the same time span, only 707 new trees were planted. However, at the time of the report, the city had just approved a plan to plant 5600 trees, replacing collapsed or unstable specimens, and adding new trees to city streets and public parks [44].

The specific region of interest (ROI) that is analyzed in this study is a 2 × 3 km rectangle, with an additional 200 m buffer applied to avoid edge effects and potential errors in subsequent processing. Various reasons have led to the selection of this specific ROI as an emblematic case for an investigation into urban tree distribution. First of all, it meets the requirements of being in an urban context characterized by a densely built environment interspersed with vegetation and a significant presence of tree cover, as shown in Figure 2 (based on an analysis by the authors using the 10 m spatial resolution ISPRA 2021 Land Cover Map [45]. The ROI is approximately 57% occupied by artificial surfaces, 19% by low vegetation, and the remaining 24% by tree vegetation). Furthermore, this area is characterized by a complex topography, with an elevation ranging from about 14 m a.s.l. to about 460 m a.s.l.

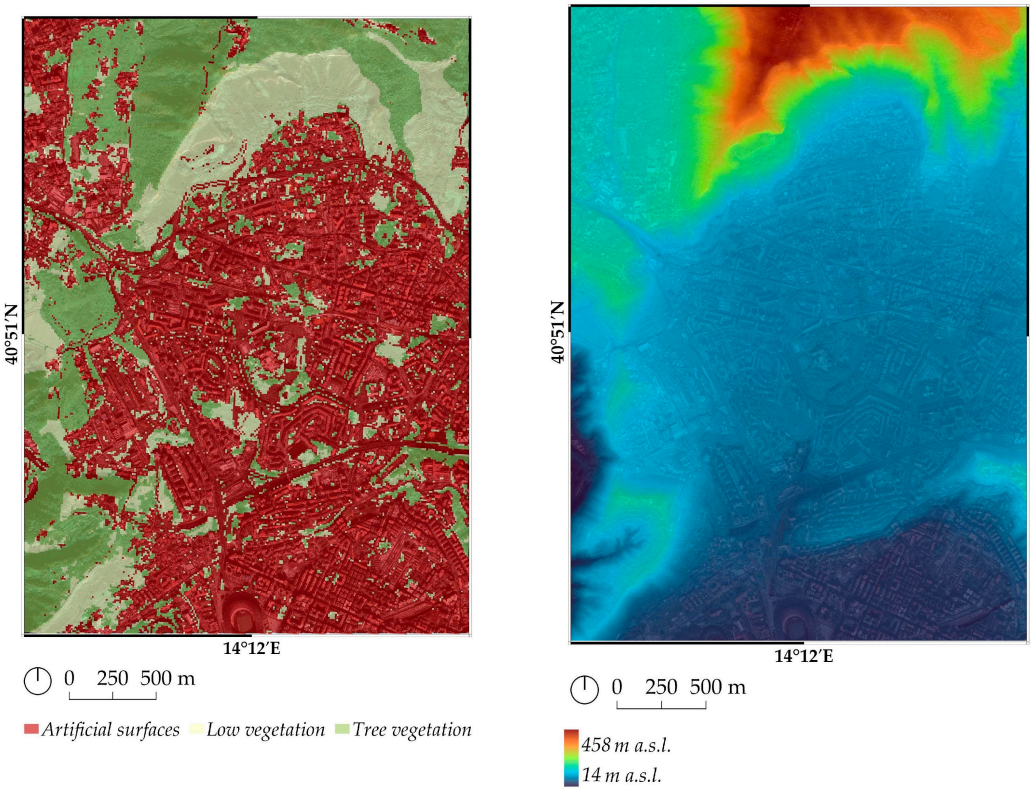

Figure 2. This figure shows the principal land cover class present and the altitude of the ROI: (**a**) using the ISPRA 2021 Land Cover Map; (**b**) using the DTM of the metropolitan city of Naples.

Finally, data coming from different sources were available for the area that could be used synchronously in order to test out the experimented classification method. In particular, for research purposes, the Public Greenery office of the Municipality of Naples made a particularly accurate forest inventory available containing the tree species present

throughout the ROI, collected between 2016 and 2022 (A. Pepe, personal communication, March 2024). This information was used as a dataset for GTs. For the same area, a very high resolution (VHR) Pléiades image acquired on 17 November 2018 is available, along with a Digital Terrain Model (DTM) and a Digital Surface Model (DSM) collected between 2009 and 2012 and distributed by the Metropolitan City of Naples [46].

The ROI is within an HSI PRISMA view acquired on 4 November 2020. From a temporal perspective, the Pléiades and PRISMA images can be considered contemporaneous with the GTs, while the information contained in the DTM and DSM is about eight years older. This time interval was deemed acceptable for distinguishing between areas with low vegetation and wooded areas. The actual presence of trees was verified through photointerpretation of the VHR image to ensure the validity of the information contained in the DSM.

2.2. Pre-Processing and Identification of the Forested Areas

The methodology used for data preparation can be divided into two separate phases. In the first phase, the Pléiades image underwent preprocessing and then was used within the ROI in combination with the DTM and DSM difference to define a clipping mask that only included wooded areas and excluded low vegetation. In the second phase, a subset of the HSI was selected, both spectrally by eliminating the bands without information, and spatially by applying step one's filter with the clipping mask of the wooded areas.

2.2.1. Multispectral Dataset

All multispectral data from the Pléiades satellite is made up of four multispectral (MS) bands (blue = 0.43–0.55 μm; green = 0.50–0.62; μm; red = 0.59–0.71 μm; near-infrared = 0.74–0.94 μm), with a spatial resolution of 2 m, and a panchromatic band with a 0.5 m resolution that covers wavelengths between 0.47 and 0.83 μm of the visible spectrum [47].

The first phase of data preparation involved preprocessing the Pléiades image acquired on 17 November 2018 using PCI Geomatica 2017 software. Atmospheric correction was performed for both the multispectral and panchromatic bands using the ATCOR module, and pansharpening was carried out using the "High Performance Image Fusion" algorithm to achieve a 0.5 m resolution and spatial enhancement of the MS bands. Orthorectification of the image was accomplished using the OrthoEngine module with Toutin's mathematical model, utilizing GCPs and the DTM of the metropolitan city of Naples with a 1 m resolution. The processed data were then clipped to the ROI, resulting in the multispectral dataset (MS_DS) used for the subsequent phase.

In the second phase, a preliminary classification of the area was performed to distinguish trees from the rest of the land cover. The availability of the VHR MS_DS was crucial for this operation because the hyperspectral data alone, with a GSD of 30 m, would pose significant scale limitations in detailing individual tree canopies. Therefore, the MS_DS was segmented using eCognition Essential 1.30 software with the Multiresolution Segmentation algorithm. The segmented areas corresponding to tree canopies were separated from other segments in two steps.

The first step involved the separation of only vegetated areas, using the normalized difference vegetation index (NDVI) and only selecting areas with NDVI > 0.2, through the Threshold Segmentation/Classification algorithm. NDVI, calculated as a ratio between near-infrared and red spectral reflectance, leverages the way photosynthesizing leaves reflect light. On land, NDVI values range from 0 to 1, where 0 indicates no plant cover, and 1 represents dense, healthy vegetation. Following [48], an NDVI threshold (>0.2) was used to detect all vegetation, including areas with lower photosynthetic activity.

The second step involved the separation of trees from grasslands and shrubs using the same algorithm but based on the normalized difference between the DSM and the DTM (nDSM) and only selecting vegetated areas with a height greater than 5 m. A DSM is a 3D model of the Earth's surface representing everything visible, including objects such as

buildings and vegetation. A DTM is a 3D representation of the Earth's surface including bare-ground topography but excluding objects such as buildings and vegetation. This difference can be used to filter images for analysis, selecting only objects above the terrain. The vector data obtained at the end of this procedure containing polygons of the wooded areas was subsequently rasterized with a spatial resolution of 0.5 m and used as a clipping mask for the hyperspectral dataset (HSI_mask). The HSI_mask is shown in Figure 3.

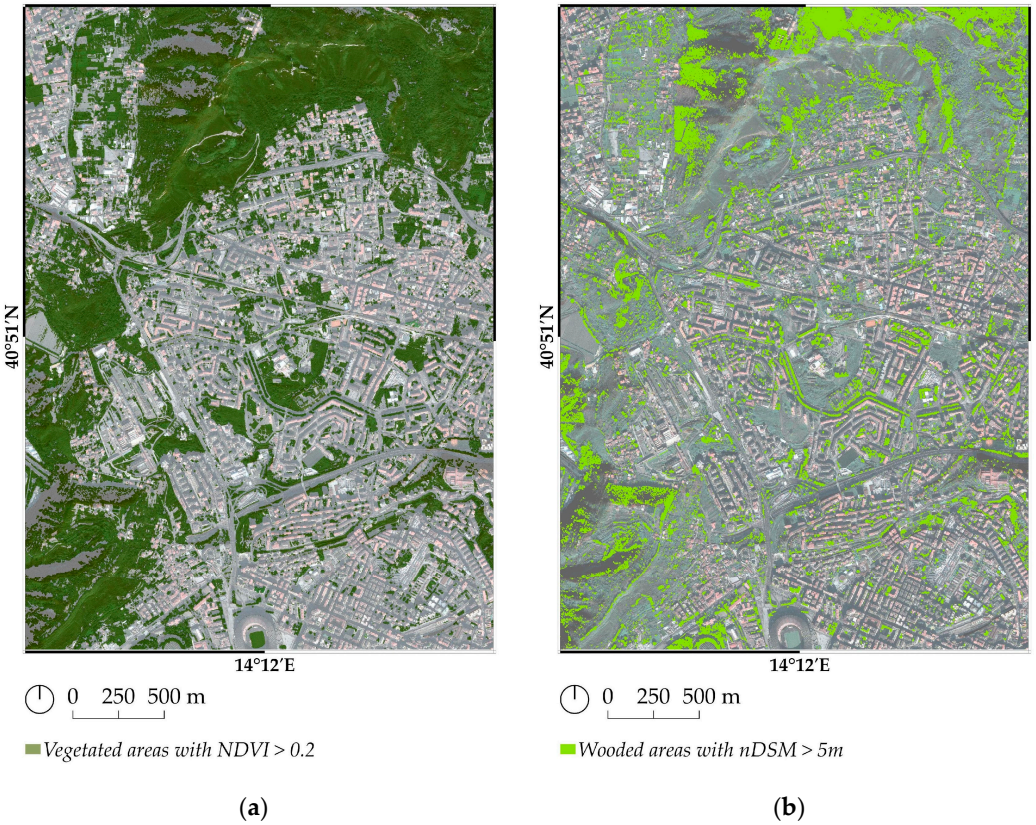

(**a**) (**b**)

Figure 3. This figure shows the main step used to separate tree canopies from other land covers using the MS Pléiades data: (**a**) map of vegetated areas with NDVI > 0.2; (**b**) map of vegetated areas higher than 5 m.

2.2.2. Hyperspectral Dataset

PRISMA data are made up of 66 bands in the visible and near-infrared (VNIR) range (400–1010 nm), 174 bands in the shortwave infrared (SWIR) range (920–2505 nm), which partially overlap, and one panchromatic (PAN) band (400–700 nm). The spatial resolution of the VNIR and SWIR is 30 m, while it is 5 m for the PAN. This study uses a level 2-D product. The data were first processed with a Python script (Prisma Tool) [49] developed by the authors and freely available.

Using the Prisma Tool, the HDF5 file provided by ASI was converted into the GeoTiff format while simultaneously improving the georeferencing of the four corners of the view. As expected from the literature, three windows in the infrared range were completely opaque due to water vapor and other atmospheric gasses, causing a low signal-to-noise ratio. Thus, the data were filtered based on a statistical analysis using R software (v. 4.4.1), by removing the bands in the intervals from 1361 nm to 1449 nm, 1803 nm to 1949 nm, and 2483 nm to 2497 nm. This resulted in a hyperspectral dataset composed of 205 bands (HS_DS).

2.2.3. Pansharpening and Subsetting

Using QGIS (v. 3.34), two separate procedures were carried out to derive two HSI datasets from the HS_DS for classification purposes. For the first HSI (HSI1), the original

spatial resolution of 30 m was maintained unaltered. For the second HSI (HSI2), the spatial resolution was increased to 5 m using the panchromatic band, as explained in detail below. Both HSIs were clipped after a precautionary buffer of 1 km was created around the ROI to avoid errors in the subsequent spatial alignment operations harmonizing the various datasets (HS1, HS2, MS_DS, HSI_mask, and GT points).

HSI1 was obtained through a simple merging of the 205 bands from the PRISMA data. To generate HSI2, four distinct steps were required. In step 1, the 36 bands in the PAN range (400–700 nm) with a GSD of 30 m were selected and merged into a single multiband raster file, keeping the value of the pixels contained in each band separate. In step 2, pansharpening was performed on the merged bands from step 1 using the PAN band as the sharpening band. This was accomplished using the GDAL library in QGIS and the Cubic resampling algorithm (4 × 4 Kernel), resulting in a new image with a GSD of 5 m. In step 3, the remaining 169 bands of the HS were merged, as in step 1, and their spatial resolution was reduced to 5 m through a downscaling operation, creating 36 new pixels for each pixel with a GSD of 30 m. In step 4, the pixel values contained in each of the original pixels with a GSD of 30 m in the 169 bands were preserved and reassigned to the 36 new pixels generated within each original pixel. The images produced in step 2 and step 4 were merged into a new multiband raster file, producing HSI2. Figure 4 shows HSI1 and HSI2 before applying the HSI_mask.

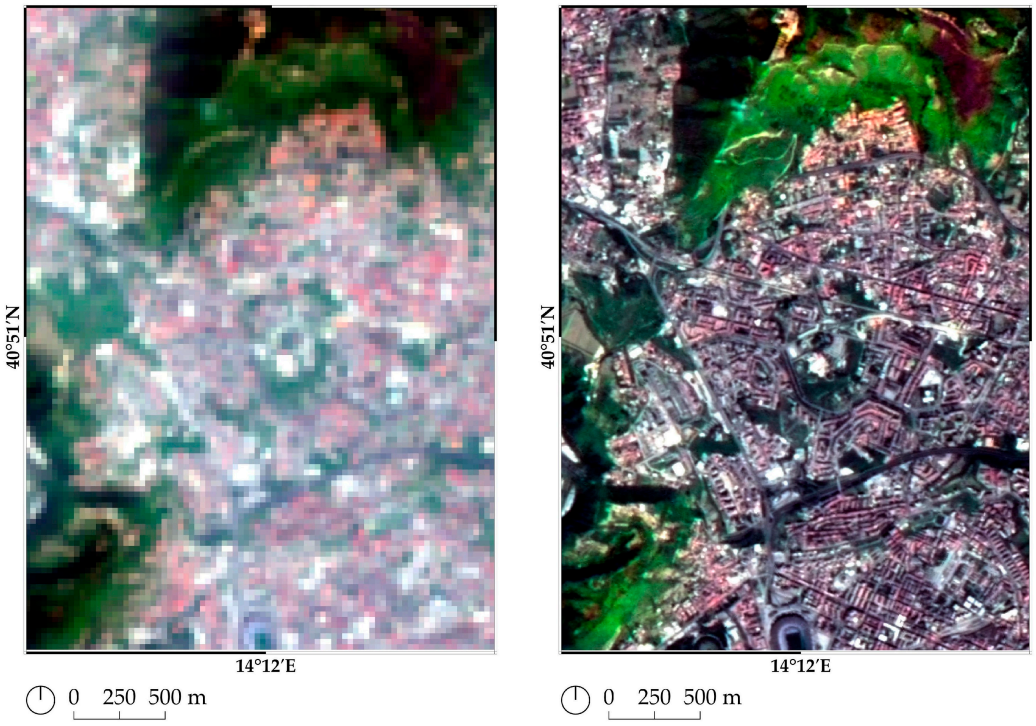

Figure 4. This figure shows the two PRISMA HSIs clipped on the ROI in natural colors: (**a**) HSI1 with 30 m spatial resolution; (**b**) HSI2 with 5 m spatial resolution.

Both HSI1 and HSI2 were subjected to a georeferencing procedure. This was carried out to align the grids of both raster images and ensure that they matched the clipping mask of the wooded areas. The operation was carried out in QGIS using Polynomial 2 as the transformation type and Nearest Neighbor as the resampling method. The GCPs used in this process were collected using the Pléiades VHR image as a reference image.

Finally, a subsetting selection of HSI1 and HSI2 was performed using the HSI_mask as a filter to remove all pixels that were not of interest for classification. In the selected subset, all HSI1 and HSI2 pixels were retained where at least 30% of the pixel area was covered by

the HSI_mask surface, and thus could be considered as corresponding to wooded areas. After trials with 40% and 50%, the 30% threshold was selected as the best trade-off for achieving good classification accuracy while retaining a high number of wooded areas or individual trees. In this way, the values for pixels in wooded areas were preserved, and the NoData class was assigned to the portions of the HSI1 and HSI2 images corresponding to areas not of interest.

2.3. Classification Task

2.3.1. Ground Truth Dataset

The municipality of Naples' Office of Public Greenery keeps a vector point database of the tree specimens located in the urban area, including street trees and trees within public parks. There are approximately 1400 points within the ROI, representing 72 different species. The main purpose of this study is to compare the classification results of HSI1 and HSI2. For this reason, it was deemed appropriate to select the species for classification based on their frequency in the GTP dataset. The five species represented by more than 50 points are listed in Table 1, with the exception of *Ligustrum lucidum*. Other species represented by less than 50 points were not included in the classification, as they were represented by an insufficient number of points to validate the results. The *Ligustrum lucidum* class was excluded due to the small size of the specimens present in the study area. Also, all of the points representing the genus *Eucalyptus* spp. (*Eucalyptus globulus*, *Eucalyptus* sp.) were grouped into a single class included in the classification.

Table 1. This table contains the number of GTPs within the ROI used as reference data for the classification task.

Species	GTPs
Pinus pinea	424
Tilia × *europaea*	310
Platanus × *acerifolia*	103
Quercus ilex	51
Eucalyptus spp.	50
Total	938

The positions of the 996 GT points were verified one by one using MS_DS as a basemap and, where necessary, the points were placed correctly on their corresponding crown. The number of labeled pixels used as reference data in the following classification procedure is a little less than the number of GT points listed in the table above and slightly varies in the classification of HSI1 and HSI2, as the values in the Supplementary Materials show. This variation is due to the rare cases in which multiple points from the GTP dataset were located within a single pixel of the 30 × 30 m grid for HSI1 or the 5 × 5 m grid for HSI2. In these rare cases, a single labeled pixel was derived from multiple GT points.

2.3.2. HSI1 and HSI2 Classification

Deep learning models were used to classify HSI1 and HSI2, as they are able to learn nonlinear features of hyperspectral data compared to traditional machine learning algorithms [50–52]. The classification of the PRISMA image was performed using a convolutional neural network (CNN) model with a structure that has been shown to be particularly suitable for land cover studies [53–55].

Specifically, the classification procedure used the plugin AVHYAS in the open-source software Qgis 3.14. The AVHYAS plugin proposes various models of CNN; in this study, the model proposed by Hu et al. was chosen for its good results working with hyperspectral data [53,56]. It consists of five layers: the first layer represents the pixel spectral vector; followed by a convolutional layer; the max pooling layer; the fully connected layer; and the output layer.

The GT points were divided into three groups with different percentages. Thirty percent of the 938 points were reserved for the final classification test and separated from the remaining 70%, which was further divided into 70% for CNN training and 30% for model validation. The random selection of points for each of the three groups was repeated in a five-fold process assigning points to the training, validation and testing phases for both HSI1 and HSI2, corresponding to ten separate classification trials. The experimentation phase was conducted in successive iterations, where, under the same conditions, different points were selected for the training, validation, and test groups, alternating the two input HSIs.

In AVHYAS, the learning rate and the number of epochs were the only parameters that were changed during CNN tuning, while the other parameters were left at their default settings. Choosing the learning rate is important because if it is too small, it can slow down the process of adjusting the network weights to find the best solution, and there is a risk of ending up in a local minimum with a non-ideal solution. Conversely, if the learning rate is too high, a search for the minimum gradient that reduces the error rate may skip the ideal solution. An ideal learning rate of 0.001 was chosen, which is one of the most widely used values in the literature [57], based on the accuracy of the obtained results. The number of epochs was set to 200, which was empirically found to be an optimal number based on the accuracy achieved during validation. However, this number sometimes turned out to be lower due to an automatic arrest of the process to avoid overfitting the data. Both HSI1 and HSI2 images were classified using the same set of GTPs in each trial.

The quality of the classification was evaluated using some of the most common accuracy metrics: Overall Accuracy (OA), Kappa Coefficient (K), User Accuracy (UA), and Producer Accuracy (PA) [58]. Additionally, the F1 score (F1) was calculated, which is a metric derived from the harmonic mean between UA and PA and is more suitable in the case of an unbalanced label dataset among the various classes [59,60].

3. Results

This section presents the results obtained from classifying the two images, HSI1 (30 m GSD) and HSI2 (GSD 5 m). At the beginning of each trial, different points were randomly assigned to the validation and test groups, separating them from the points used for training. Specifically, the percentages of the 938 points allocated to the three different groups are: 30% for the final test of the results, 49% for training the CNN, and 21% for validating the classification model. In this way, two confusion matrices were generated for each trial, one for validation and one for testing, from which the accuracy metrics were measured. The twenty confusion matrices generated from the five trials are included in the Supplementary Materials along with the OA, K, UA, PA, and F1 values. For brevity, this section only reports the values related to the test phase of the results, which is deemed most representative of the trials conducted.

Table 2 contains the OA and the inter-rater reliability K coefficient obtained for every trial (T) relative to the test phase. The OA ranges in the results in the last row show that, on average, HSI2 achieves an accuracy value that is 0.14 points higher compared to HSI1. Similarly, the K values show an inter-rater reliability coefficient of 0.2 higher for the HSI2 image that has undergone pansharpening.

UA and PA are very useful for assessing the underestimation or overestimation of individual classes [58]. They complement commission error and omission error metrics. The values of these metrics for each test in the validation phase and in the test phase are shown in the Supplementary Materials. Table 3 shows the average value of UA and PA obtained in the test phase for all the trials performed with HSI1 and for all the trials performed with HSI2. In general, it is evident that the UA and PA values increase when the HSI2 image is used. The reasons for this improvement are related to the application of the pansharpening technique and will be discussed below. One aspect that must be emphasized here is that with the use of the HSI2 image, there is a reduction in both inclusion errors (commission errors) and exclusion errors (omission errors). This is driven by a substantial

increase in both UA and PA. In fact, for the classes *Pinus pinea* and *Tilia* × *europaea*, for which the PA values are slightly higher than the UA values, the HSI2 image makes it possible to reduce the commission error margin, thus reducing the overestimation. For the other classes, where the UA values are greater than the PA values and thus underestimation occurs, a reduction in the omission error is obtained compared to the use of HSI1. The classes *Pinus pinea* and *Tilia* × *europaea* are slightly overestimated, while all the other classes are underestimated, using both HSI1 and HSI2. This phenomenon is probably related to the number of GTs, which is higher for *Pinus pinea* and *Tilia* × *europaea*, allowing a higher representativeness and avoiding the omission error.

Table 2. This table relates to the test phase and shows the OA and K values obtained for every trial (T), the relative average values for each HSI and the interval between HSI1 and HSI2 metric averages.

			OA			
	T1	T2	T3	T4	T5	Av.
HSI1	0.65	0.67	0.65	0.60	0.61	**0.64**
HSI2	0.83	0.82	0.74	0.79	0.74	**0.78**
Interval						**0.14**
			K			
	T1	T2	T3	T4	T5	Av.
HSI1	0.48	0.47	0.46	0.32	0.34	**0.41**
HSI2	0.74	0.72	0.59	0.67	0.59	**0.66**
Interval						**0.25**

Table 3. This table refers to the test phase and shows the average values of UA and PA. The average is calculated for the 5 trials using HSI1 and the 5 trials using HSI2.

Species	**HSI1**		**HSI2**	
	UA	**PA**	**UA**	**PA**
Pinus pinea	0.65	0.88	0.79	0.89
Tilia × *europaea*	0.63	0.67	0.84	0.86
Platanus × *acerifolia*	0.31	0.11	0.68	0.60
Quercus ilex	0.27	0.12	0.35	0.27
Eucalyptus spp.	0.56	0.14	0.82	0.34

Table 4 shows the results in terms of F1 related to the test phase of the five classification trials (T) conducted using the two images, HSI1 and HSI2. Furthermore, the table shows the average F1 obtained per class, along with the range that indicates the improvement generated by the use of pansharpening. The improved accuracy of the results demonstrates the effectiveness of pansharpening. With the higher resolution of the HSI2 image, the classifier can more accurately identify the spectral signature of tree species and assign pixels to the correct class. In contrast, the lower resolution of the HSI1 image makes this task more challenging, complicating the classification process. The pansharpening method makes it possible to emphasize the spectral characteristics of surfaces, even if only in the panchromatic range, by sharpening the values contained in the lower resolution pixels without altering the shape of the spectral signatures' curve. This makes it possible to distinguish pixels containing a mixed signature from several materials.

Table 4. This table refers to the test phase and shows the F1 values by class obtained with HSI1 and HSI2 in each trial (T), the relative average values for each HSI and the interval between HSI1 and HSI2 metric averages.

Species	HSI1 (F1)						HSI2 (F1)						
	T1	T2	T3	T4	T5	Av.	T1	T2	T3	T4	T5	Av.	Interval
Pinus pinea	0.75	0.78	0.74	0.71	0.73	**0.74**	0.86	0.86	0.81	0.83	0.81	**0.84**	**0.10**
Tilia × *europaea*	0.68	0.69	0.65	0.61	0.60	**0.65**	0.89	0.86	0.84	0.86	0.79	**0.85**	**0.20**
Platanus × *acerifolia*	0.40	0.22	0.00	0.00	0.14	**0.15**	0.75	0.79	0.32	0.68	0.62	**0.63**	**0.48**
Quercus ilex	0.41	0.00	0.00	0.00	0.18	**0.12**	0.50	0.47	0.11	0.29	0.00	**0.27**	**0.15**
Eucalyptus spp.	0.40	0.50	0.00	0.15	0.00	**0.21**	0.64	0.40	0.53	0.48	0.25	**0.46**	**0.25**

The fluctuations in F1 across the different trials show how the selection of GTPs for testing can lead to varying results, especially when the test is conducted with a relatively small number of points. The columns of average values indicate that higher F1s are achieved for classes with a greater number of GTPs. Even in cases where the F1 remains at very low thresholds, a substantial improvement can still be observed following pansharpening with HSI2, as evident from the last column. The classification results of all experiments with HSI1 and HSI2 are shown in Figure 5.

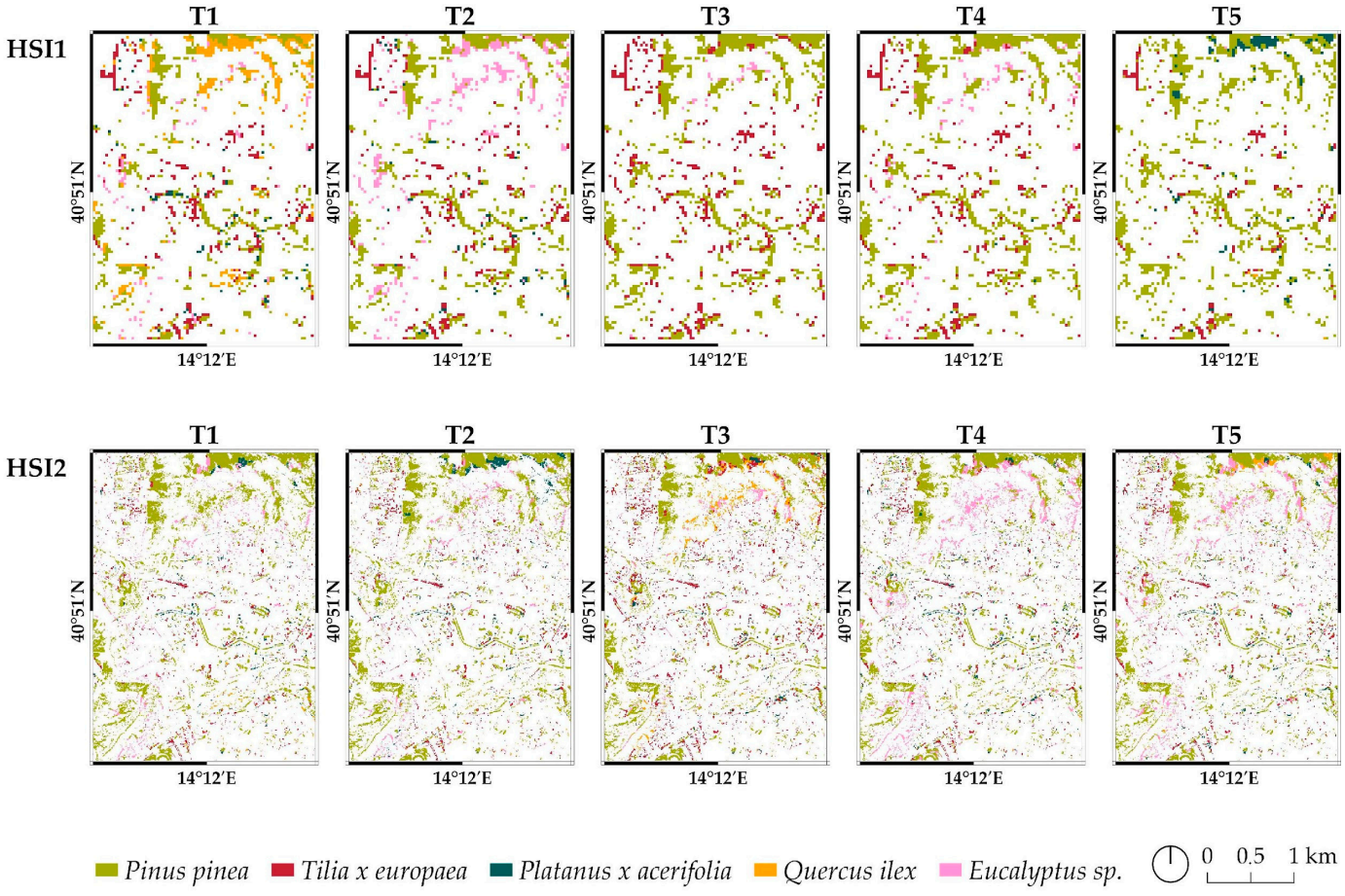

Figure 5. Classification results obtained in all trials (T) using HSI1 and HSI2.

4. Discussion

The investigation's results demonstrate that the direct use of pansharpening by taking advantage of the coregistered panchromatic data can lead to excellent classification results (OA from 0.64 to 0.78) in urban areas with complex topography, dense settlement patterns,

and fragmented green areas [45]. The UA and PA values can be increased, and both the commission error and the omission error can be reduced by using the improved hyperspectral data. The result is an improvement in the reliability of the classification map.

These key findings clearly show that the operation alone significantly improves the quality of the classification, given that the same conditions and software are used. For the classes under investigation with a larger number of GTs, the F1 value increased on average from 0.74 to 0.84 for the *Pinus pinea* class, and even more significantly went from 0.65 to 0.85 for the *Tilia* × *europaea* class. The classification of these two species benefits from a high number of GTs, and therefore the results confirm the efficiency of the proposed method. It can be stated that the application of pansharpening in an urban environment can lead to a considerable improvement in classification accuracy. Although other species with fewer GTs show even more pronounced improvements, these are less significant due to the smaller sample size of GTs.

The improved accuracy metrics (OA, K, UA, PA, and F1) show that pansharpening can be an affordable alternative for high spatial resolution hyperspectral data. The proposed method enhances spatial resolution by applying pansharpening to the hyperspectral bands in the range covered by the panchromatic band (400–700 nm), leaving the values recorded by the hyperspectral sensor in the other bands unchanged. The reconstruction of the details of the spectral signature and the spatial patterns is definitely more effective with the use of multispectral data over several intervals of the spectrum (De Luca, 2024 [39]). However, the pansharpening operation allowed the spatial distribution of the different surfaces to be highlighted without altering the shape of the spectral signature curve, especially in the mixed pixels of the 30 m resolution data. This process resulted in a better distinction of the spectral signature of the studied classes and improved classification accuracy. Thus, to improve the spatial resolution of the data without using laborious techniques, pansharpening the PRISMA data with the coregistered panchromatic band is a viable and accessible option.

One of the most promising applications of remote sensing technology is environmental resource and biodiversity monitoring. Research has been conducted evaluating the accuracy of image classification based on various data sources, including very high resolution imagery, nDSM, and HSI [2,11]. Recent advancements in spectroscopy satellite missions, such as PRISMA, have made this last option much more accessible. However, existing open-access satellites provide images at a relatively coarse resolution (30 m or lower), which works quite well in larger natural environments [34]. However, a finer resolution is necessary in urban environments where images are typically composed of spectrally mixed pixels [35], and canopies are fragmented and often made up of different species grouped close together [2].

Satellite HSIs typically have a spatial resolution of about 30 m and consist primarily of spectrally mixed pixels in urban contexts [35]. Hyperspectral data with higher spatial resolution can be acquired from airplane field missions with sensors such as CASI with a 2–5 m spatial resolution, depending on altitude [27], or restricted access satellite missions, such as TacSat-3 with a 4 m spatial resolution [61]. However, both of these sources pose data availability and accessibility problems for entities involved in biodiversity monitoring (government bodies, universities, non-profit organizations, etc.). Airplane missions only capture a small field of view and private or military high-resolution satellites are either too costly or too classified to be acquired. Thus, HSI remains one of the best options, if it can be refined to a higher resolution.

Viable techniques to address these limitations and enhance HSI for urban classification include pansharpening and hypersharpening, which improve spatial resolution by fusing data with higher-resolution sources. In fact, the validity of the pansharpening or hypersharpening methods to enhance HSI data from PRISMA while preserving the original spectral characteristics has been demonstrated [39] by comparing the enhancement result with hyperspectral data acquired at the origin from higher resolution aircraft sensors

(CASI/SASI). However, each one of these techniques has advantages and drawbacks. This study availed itself of pansharpening for the specific reasons explained below.

Research shows that using pansharpening to adjust the reflectance of hyperspectral data improves the spatial resolution of the new pixels. However, this process only adjusts the intensity of the hyperspectral signature based on the panchromatic information, without adding any new radiometric information [38,39,41]. Approaches proposed in other studies [37–39], which use hypersharpening with Sentinel data, would likely yield even more accurate results, particularly in flat areas where orthorectification of non-coregistered images is less challenging. In such a context, Hypersharpening may have some additional potential compared to single-band pansharpening.

Hypersharpening regards the fusion of higher spatial resolution multispectral data with hyperspectral data. Each of the multispectral bands is used as a sharpening band, as opposed to pansharpening, where only the panchromatic band is used. Hypersharpening allows the corresponding hyperspectral bands to be grouped using the wavelength range of each multispectral band. Hyperspectral enhancement is thus determined as a function of the values recorded by the multispectral sensor in different spectral regions, instead of just once for the entire panchromatic range, as in pansharpening.

However, while this technique certainly has advantages in terms of spectral signature reconstruction, it also has drawbacks. These are related to the use of scenes acquired by different satellites, at different times, at different angles, and using a mismatched orthorectification. This method relies on images taken from different satellites in different moments and thus demands high precision in orthorectification to prevent spatial misalignments and the overlapping of acquisition dates. Additionally, radiometric differences—due to factors like noise, sensor sensitivity, and atmospheric correction—can occur even for data captured on the same day [39].

The pansharpening method proposed in this study uses a coregistered image to simplify processing, principally because the images are taken simultaneously, thereby avoiding the need for overlapping acquisition dates and complicated preprocessing (geocoding and the spatial alignment of the two datasets). Thus, it is the more practical choice for biodiversity monitoring in urban contexts.

5. Conclusions

This study aimed to achieve both a technical and a practical objective: to evaluate the contribution of pansharpening to improve image classification accuracy using hyperspectral data, so that it is also useful in urban settings; and, to apply this method to a real-world problem, specifically urban tree monitoring, through a simple pansharpening application that only uses the more easily accessible panchromatic band. In order to carry out these objectives, the classification accuracy results for some tree species obtained with HSI1 (GSD 30 m) and HSI2 (GSD 5 m) were compared. The results showed that pansharpening improves classification quality in dense urban areas with complex topography. In fact, pansharpened data led to significantly higher classification accuracy for all the examined species.

Through its investigation, this study made contributions by:

- introducing a novel application using pansharpening techniques to improve classification performance in urban environments by enhancing the spatial resolution of PRISMA hyperspectral imaging data;
- demonstrating its efficiency by applying the method to a practical real-world use of pansharpened image classification for urban tree monitoring.

Thus, dissemination of this method could improve HSI classification performance to help public administrations that are currently struggling to meet international and national policy demands to monitor biodiversity at various scales of governance.

In fact, the study's results confirm one of the objectives of the PRISMA mission, which is intended as a precursor to the applied mission: to evaluate the benefits of using coregistered panchromatic data [30,42]. To the best of our knowledge, there are no specific evaluations of pansharpening for PRISMA data based on the use of GTs for classification

purposes in urban environments. Based on the results of this initial study, it could be said that the PRISMA mission has confirmed the usefulness of a panchromatic band sensor on hyperspectral satellite platforms.

Based on these findings, the following recommendations can be made. Firstly, it seems that hyperspectral data have potential to be used to differentiate the spectral signatures of trees in complex urban environments. Indeed, this technique addresses the needs of public administrations seeking to follow international and national urban forestry policies, recognizing the many contributions made by urban trees to health and wellbeing, ecosystem functions, biodiversity conservation, and sustainable development. In Italy, national legislation such as the *Regulations for the Development of Urban Green Spaces* (Italian Law n. 10, 14 January 2013) [62] and the *Minimum Environmental Criteria (CAM) for Public Green Space Management Services and the Supply of Green Care Products* (Ministerial decree n. 63 of 10 March 2020) [63] require municipal administrations to keep up-to-date georeferenced tree inventories specifying the number, species, health, and location of specimens and a plan for their management. This study was fortunate enough to be able to make use of an extensive inventory provided by the Public Greenery Department of the municipality of Naples. However, not all cities are able to keep up with policy demands. In fact, the same CAM legislation mentioned above was conceived to nudge municipalities into compliance by making up-to-date tree inventories and management plans a mandatory step in public procurement processes. The problem regards the limited number of public employees with the specialized skills necessary to create and update such an inventory and the huge amount of time such a feat requires. The approach proposed by this study could clearly be of great use to speed up this enterprise. By using hyperspectral data for initial classification, it is possible to provide a preliminary classification and then have field personnel focus solely on verifying changes over time, which can be identified using GIS techniques. Furthermore, the collection of GTs presents an interesting opportunity for municipalities to involve other stakeholders, such as educational institutions, associations, and citizens [64].

This study's limitations are related to its focus on verifying the utility of pansharpening on PRISMA data by classifying tree species in an urban environment. While it successfully demonstrated that hyperspectral data with a 30 m resolution is useful not only in the field of forestry but also in urban areas, it was constrained by the availability of spaceborne hyperspectral data. Although easier to obtain than the other sources mentioned above, it still remains challenging for interested parties to acquire usable images in their ROI, under the conditions that they require (season, cloud cover, etc.). There is currently a very high demand for image acquisitions from users and a concentration of requests limiting the frequency of data availability [65]. The high demand for image acquisitions often makes it difficult to request new data as many users must wait their turn according to their priority status.

Future investigations could certainly start from the classification and spatial distribution of species carried out here and look more in depth at such phenomena as fragmentation and ecological connectivity in urban environments [48]. Furthermore, the obtained results suggest that future analyses could identify individual species to uncover specific vegetation characteristics and detect potential diseases. Such an approach would likely yield statistically significant results and could provide a valuable foundation for urban, peri-urban, and rural forest inventories. Furthermore, hyperspectral data could be used to compare specimens of the same species that are in different contexts in order to study phenological differences, or health status in urban environments or as a response to climate change.

Today's environmental, climate, and biodiversity challenges require innovative solutions that can be implemented at various scales with limited resources. Technologies like remote sensing and AI offer precise tools for monitoring and management. International policies, such as Agenda 2030 and the Sustainable Development Goals, increasingly rely on data-driven and adaptive management approaches. PRISMA and other hyperspectral satellite missions can significantly contribute to these global efforts by providing data that, when enhanced through techniques such as pansharpening, become more applicable in

urban environments. For effective urban tree management and improved policy implementation, it is crucial to leverage such advancements to ensure accurate, efficient, and actionable environmental monitoring.

Supplementary Materials: The following supporting information can be downloaded at: https://www.mdpi.com/article/10.3390/rs16193730/s1, File S1: Error matrices with accuracy metrics calculated for trial 1 to 5 using HSI1 and HSI2.

Author Contributions: Conceptualization, M.P., G.D., C.F., A.P., E.C. and L.B.; methodology, M.P., G.D., C.F. and L.B.; software, M.P., G.D. and L.B.; validation, M.P., G.D., C.F., A.P. and E.C.; formal analysis, M.P. and G.D.; investigation, M.P. and G.D.; resources, M.P., G.D. and L.B.; data curation, M.P. and G.D.; writing—original draft preparation, M.P., G.D. and C.F.; writing—review and editing, M.P., G.D. and C.F.; visualization, M.P.; supervision, L.B.; project administration, L.B.; funding acquisition, L.B. All authors have read and agreed to the published version of the manuscript.

Funding: This paper is part of the National Biodiversity Future Center (NBFC) project, funded under the National Recovery and Resilience Plan (NRRP). This project's study area includes some sampling areas that have been studied as part of the NBFC Spoke 5: Activity 5 "Impacts of land use and forestry actions on supporting regulating ecosystem services: biological level"; task 5.1 "Plant Reproduction in the urban environment". This research was funded under the National Recovery and Resilience Plan (NRRP), Mission 4, Component 2, Investment 1.4—Call for tender No. 3138 of 16 December 2021, rectified by Decree n.3175 of 18 December 2021 of the Italian Ministry of University and Research funded by the European Union—NextGenerationEU. Award Number: Project code CN_00000033, Concession Decree No. 1034 of 17 June 2022, adopted by the Italian Ministry of University and Research, CUP, H43C22000530001, project title "National Biodiversity Future Center—NBFC" (M.P., L.B.); the research was also partially funded by Project PRIN 2020, Sector ERC LS9 Call 2020 Prot. 2020 EMLWTN, CUP J83C20001990005 (G.D., E.C.); the research was carried out within the framework of the Ministry of University and Research (MUR) initiative "Departments of Excellence" (Law 232/2016), DIARC Project: "Habit—Inhabiting the Transition for rural constructions and agro-forestry territory" (C.F.) and DAFNE Project 2023-27: "Digital, Intelligent, Green and Sustainable (D.I.Ver.So)" (A.P.).

Data Availability Statement: Data are available with a reasonable request. Please contact the authors at the following addresses: lorenzo.boccia@unina.it or gabriele.delogu@unitus.it.

Acknowledgments: The authors would like to thank the Greenery Office of the Municipality of Naples, in particular the director Teresa Bastia and the forest agronomist Antonio Pepe, for the supply of the ground truth dataset and for the assistance in updating it in the study area.

Conflicts of Interest: The authors declare no conflicts of interest.

Abbreviations

ASI	Agenzia Spaziale Italiana (Italian Space Agency)
CAM	Criteri Ambientali Minimi (Minimum Environmental Criteria)
CNN	Convolutional Neural Network
DSM	Digital Surface Model
DTM	Digital Terrain Model
EnMAP	Environmental Mapping And Analysis Program
F1	F1 Score
GCPs	Ground Control Points
GSD	Ground Sampling Distance
GTs	Ground Truths
HS_DS	Hyperspectral Dataset with 205 bands
HSI	Hyperspectral Imagery
HSI1	Hyperspectral Imagery with GSD = 30 m
HSI2	Hyperspectral Imagery with GSD = 5 m
HSI_mask	Mask of Hyperspectral Dataset
K	Cohen's Kappa Coefficient

MS	Multispectral
MS_DS	Multispectral Dataset—Pléiades
NBFC	National Biodiversity Future Center
nDSM	Normalized Digital Surface Model
NRRP	National Recovery and Resilience Plan
OA	Overall Accuracy
PA	Producer's Accuracy
PAN	Panchromatic
PRISMA	PRecursore IperSpettrale della Missione Operativa (Hyperspectral Precursor of the Application Mission)
ROI	Region of Interest
RS	Remote Sensing
SDG	United Nations Sustainable Development Goal
SWIR	Short-Wavelength Infrared
T	Trial
UA	User Accuracy
VHR	Very High Resolution
VNIR	Visible and Near-Infrared

References

1. *United Nations World Urbanization Prospects: The 2018 Revision—United Nations Department of Economic and Social Afftair*; United Nations: New York, NY, USA, 2019; ISBN 978-92-1-004314-4. Available online: https://www.un-ilibrary.org/content/books/9789210043144/ (accessed on 7 October 2024).
2. Alonzo, M.; Bookhagen, B.; Roberts, D.A. Urban Tree Species Mapping Using Hyperspectral and Lidar Data Fusion. *Remote Sens. Environ.* **2014**, *148*, 70–83. [CrossRef]
3. Gouldson, A.; Colenbrander, S.; Sudmant, A.; Papargyropoulou, E.; Kerr, N.; McAnulla, F.; Hall, S. Cities and Climate Change Mitigation: Economic Opportunities and Governance Challenges in Asia. *Cities* **2016**, *54*, 11–19. [CrossRef]
4. Laino, E.; Iglesias, G. Extreme Climate Change Hazards and Impacts on European Coastal Cities: A Review. *Renew. Sustain. Energy Rev.* **2023**, *184*, 113587. [CrossRef]
5. Fu, J.; Dupre, K.; Tavares, S.; King, D.; Banhalmi-Zakar, Z. Optimized Greenery Configuration to Mitigate Urban Heat: A Decade Systematic Review. *Front. Archit. Res.* **2022**, *11*, 466–491. [CrossRef]
6. Tanoori, G.; Soltani, A.; Modiri, A. Predicting Urban Land Use and Mitigating Land Surface Temperature: Exploring the Role of Urban Configuration with Convolutional Neural Networks. *J. Urban Plan. Dev.* **2024**, *150*, 04024029. [CrossRef]
7. Verde, S.; Dell'Acqua, F.; Losasso, M. Environmental Data, Modeling and Digital Simulation for the Evaluation of Climate Adaptation and Mitigation Strategies in the Urban Environment. *Sustainability* **2024**, *16*, 2179. [CrossRef]
8. Dian, Y.; Pang, Y.; Dong, Y.; Li, Z. Urban Tree Species Mapping Using Airborne LiDAR and Hyperspectral Data. *J. Indian Soc. Remote Sens.* **2016**, *44*, 595–603. [CrossRef]
9. Nowak, D.J.; Hirabayashi, S.; Bodine, A.; Greenfield, E. Tree and Forest Effects on Air Quality and Human Health in the United States. *Environ. Pollut.* **2014**, *193*, 119–129. [CrossRef]
10. Malkoç, E. City-Wide Assessment of Urban Tree Cover and Land-Cover Changes in Edirne Using Web-Based Tools. *Int. J. Appl. Earth Obs. Geoinf.* **2024**, *132*, 103997. [CrossRef]
11. Morin, E.; Herrault, P.-A.; Guinard, Y.; Grandjean, F.; Bech, N. The Promising Combination of a Remote Sensing Approach and Landscape Connectivity Modelling at a Fine Scale in Urban Planning. *Ecol. Indic.* **2022**, *139*, 108930. [CrossRef]
12. Valeri, S.; Zavattero, L.; Capotorti, G. Ecological Connectivity in Agricultural Green Infrastructure: Suggested Criteria for Fine Scale Assessment and Planning. *Land* **2021**, *10*, 807. [CrossRef]
13. Mullaney, J.; Lucke, T.; Trueman, S.J. A Review of Benefits and Challenges in Growing Street Trees in Paved Urban Environments. *Landsc. Urban Plan.* **2015**, *134*, 157–166. [CrossRef]
14. Thompson, E.; Herian, M.; Rosenbaum, D. *The Economic Footprint and Quality-of-Life Benefits of Urban Forestry in the United States*; University of Nebrasca—Lincoln: Lincoln, NE, USA, 2021; pp. 1–89.
15. Pretzsch, H.; Moser-Reischl, A.; Rahman, M.A.; Pauleit, S.; Rötzer, T. Towards Sustainable Management of the Stock and Ecosystem Services of Urban Trees. From Theory to Model and Application. *Trees* **2023**, *37*, 177–196. [CrossRef]
16. United Nations Economic Commission for Europe. *Sustainable Urban and Peri-Urban Forestry: An Integrative and Inclusive Nature-Based Solution for Green Recovery and Sustainable, Healthy and Resilient Cities*; UNECE: Geneva, Switzerland, 2021; pp. 1–21.
17. Sustainable Cities and Communities—Goal 11. Available online: https://sdgs.un.org/goals/goal11 (accessed on 1 August 2024).
18. *New Urban Agenda: H III: Habitat III: Quito 17-20 October 2016*; United Nations (UN): Quito, Ecuador, 2017; ISBN 978-92-1-132731-1.
19. CREA Giornata Internazionale Delle Foreste: Verso l'Inventario Nazionale 2025—Giornata Internazionale Delle Foreste: Verso l'Inventario Nazionale 2025—CREA. Available online: https://www.crea.gov.it/en/-/giornata-internazionale-delle-foreste-verso-l-inventario-nazionale-2025 (accessed on 23 July 2024).
20. Urban Environment and Health—NBFC. Available online: https://www.nbfc.it/en/environments (accessed on 31 July 2024).

21. Cena, H.; Labra, M. Biodiversity and Planetary Health: A Call for Integrated Action. *Lancet* **2024**, *403*, 1985–1986. [CrossRef]
22. Fabbrini, F. Italy's National Recovery and Resilience Plan: Context, Content and Challenges. *J. Mod. Ital. Stud.* **2022**, *27*, 658–676. [CrossRef]
23. Comune di Napoli Manutenzione del Verde ed Igiene Della Città. Available online: https://www.comune.napoli.it/flex/cm/pages/ServeBLOB.php/L/IT/IDPagina/47672 (accessed on 1 August 2024).
24. Vihervaara, P.; Auvinen, A.-P.; Mononen, L.; Törmä, M.; Ahlroth, P.; Anttila, S.; Böttcher, K.; Forsius, M.; Heino, J.; Heliölä, J.; et al. How Essential Biodiversity Variables and Remote Sensing Can Help National Biodiversity Monitoring. *Glob. Ecol. Conserv.* **2017**, *10*, 43–59. [CrossRef]
25. Casavecchia, S.; Allegrezza, M.; Biondi, E.; Galli, A.; Marcheggiani, E.; Pesaresi, S.; Taffetani, F.; Tavoletti, S.; Zitti, S.; Bianchelli, M.; et al. Conservation and Management of Biodiversity and Landscapes: A Challenge in the Era of Global Change. In *The First Outstanding 50 Years of "Università Politecnica delle Marche": Research Achievements in Life Sciences*; Longhi, S., Monteriù, A., Freddi, A., Aquilanti, L., Ceravolo, M.G., Carnevali, O., Giordano, M., Moroncini, G., Eds.; Springer International Publishing: Cham, Switzerland, 2020; pp. 483–503. ISBN 978-3-030-33832-9.
26. Filchev, L. Satellite Hyperspectral Earth Observation Missions—A Review. *Aerosp. Res. Bulg.* **2014**, *26*, 191–207.
27. Qian, S.-E. Hyperspectral Satellites, Evolution, and Development History. *IEEE J. Sel. Top. Appl. Earth Obs. Remote Sens.* **2021**, *14*, 7032–7056. [CrossRef]
28. Caporusso, G.; Ettore, L.; Rino, L.; Rosa, L.; Rocchina, G.; Girolamo, D.M.; Patrizia, S. The Hyperspectral Prisma Mission in Operations. In Proceedings of the IGARSS 2020—2020 IEEE International Geoscience and Remote Sensing Symposium, Waikoloa, HI, USA, 26 September–2 October 2020; IEEE: Waikoloa, HI, USA, 2020; pp. 3282–3285.
29. Storch, T.; Honold, H.-P.; Chabrillat, S.; Habermeyer, M.; Tucker, P.; Brell, M.; Ohndorf, A.; Wirth, K.; Betz, M.; Kuchler, M.; et al. The EnMAP Imaging Spectroscopy Mission towards Operations. *Remote Sens. Environ.* **2023**, *294*, 113632. [CrossRef]
30. Cogliati, S.; Sarti, F.; Chiarantini, L.; Cosi, M.; Lorusso, R.; Lopinto, E.; Miglietta, F.; Genesio, L.; Guanter, L.; Damm, A.; et al. The PRISMA Imaging Spectroscopy Mission: Overview and First Performance Analysis. *Remote Sens. Environ.* **2021**, *262*, 112499. [CrossRef]
31. Guanter, L.; Kaufmann, H.; Segl, K.; Foerster, S.; Rogass, C.; Chabrillat, S.; Kuester, T.; Hollstein, A.; Rossner, G.; Chlebek, C.; et al. The EnMAP Spaceborne Imaging Spectroscopy Mission for Earth Observation. *Remote Sens.* **2015**, *7*, 8830–8857. [CrossRef]
32. Fassnacht, F.E.; Latifi, H.; Stereńczak, K.; Modzelewska, A.; Lefsky, M.; Waser, L.T.; Straub, C.; Ghosh, A. Review of Studies on Tree Species Classification from Remotely Sensed Data. *Remote Sens. Environ.* **2016**, *186*, 64–87. [CrossRef]
33. Dalponte, M.; Bruzzone, L.; Gianelle, D. Tree Species Classification in the Southern Alps Based on the Fusion of Very High Geometrical Resolution Multispectral/Hyperspectral Images and LiDAR Data. *Remote Sens. Environ.* **2012**, *123*, 258–270. [CrossRef]
34. Vangi, E.; D'amico, G.; Francini, S.; Giannetti, F.; Lasserre, B.; Marchetti, M.; Chirici, G. The New Hyperspectral Satellite Prisma: Imagery for Forest Types Discrimination. *Sens. Switz.* **2021**, *21*, 1182. [CrossRef] [PubMed]
35. Rosentreter, J.; Hagensieker, R.; Okujeni, A.; Roscher, R.; Wagner, P.D.; Waske, B. Subpixel Mapping of Urban Areas Using EnMAP Data and Multioutput Support Vector Regression. *IEEE J. Sel. Top. Appl. Earth Obs. Remote Sens.* **2017**, *10*, 1938–1948. [CrossRef]
36. Palsson, B.; Sigurdsson, J.; Sveinsson, J.R.; Ulfarsson, M.O. Hyperspectral Unmixing Using a Neural Network Autoencoder. *IEEE Access* **2018**, *6*, 25646–25656. [CrossRef]
37. Acito, N.; Diani, M.; Corsini, G. PRISMA Spatial Resolution Enhancement by Fusion With Sentinel-2 Data. *IEEE J. Sel. Top. Appl. Earth Obs. Remote Sens.* **2022**, *15*, 62–79. [CrossRef]
38. Alparone, L.; Arienzo, A.; Garzelli, A. Spatial Resolution Enhancement of Satellite Hyperspectral Data Via Nested Hyper-Sharpening With Sentinel-2 Multispectral Data. *IEEE J. Sel. Top. Appl. Earth Obs. Remote Sens.* **2024**, *17*, 10956–10966. [CrossRef]
39. De Luca, G.; Carotenuto, F.; Genesio, L.; Pepe, M.; Toscano, P.; Boschetti, M.; Miglietta, F.; Gioli, B. Improving PRISMA Hyperspectral Spatial Resolution and Geolocation by Using Sentinel-2: Development and Test of an Operational Procedure in Urban and Rural Areas. *ISPRS J. Photogramm. Remote Sens.* **2024**, *215*, 112–135. [CrossRef]
40. PRISMA Algorithm Theoretical Basis Document (ATBD). Available online: https://prisma.asi.it/missionselect/docs/ (accessed on 30 July 2024).
41. Alparone, L.; Aiazzi, B.; Baronti, S.; Garzelli, A. Remote Sensing Image Fusion. In *Remote Sensing Image Fusion*; CRC Press: Boca Raton, FL, USA, 2015; p. 178. ISBN 978-0-429-16822-2.
42. Galeazzi, C.; Carpentiero, R.; Varacalli, G. The Prisma System and PAN/HYP Instrument. In Proceedings of the 6th EARSeL Imaging Spectroscopy SIG (Special Interest Group) Workshop, Tel Aviv, Israel, 16–18 March 2009; p. 10.
43. ISTAT Istat Data. Available online: https://esploradati.istat.it/databrowser/#/en/dw (accessed on 20 September 2024).
44. Comune di Napoli Bilancio Arboreo e Gestione del Verde Della Città di Napoli. Available online: https://www.comune.napoli.it/flex/cm/pages/ServeBLOB.php/L/IT/IDPagina/29726 (accessed on 1 August 2024).
45. ISPRA Uso Del Suolo 2021 | Uso, Copertura e Consumo Di Suolo. Available online: https://groupware.sinanet.isprambiente.it/uso-copertura-e-consumo-di-suolo/library/copertura-del-suolo/carta-di-copertura-del-suolo/uso-del-suolo-2021 (accessed on 1 August 2024).
46. Città Metropolitana Di Napoli—SIT. Available online: https://sit.cittametropolitana.na.it/ (accessed on 2 August 2024).
47. Perko, R.; Raggam, H.; Schardt, M.; Roth, P.M. Very High Resolution Mapping with the Pléiades Satellite Constellation. *Am. J. Remote Sens.* **2018**, *6*, 89–99. [CrossRef]

48. Casalegno, S.; Anderson, K.; Cox, D.T.C.; Hancock, S.; Gaston, K.J. Ecological Connectivity in the Three-Dimensional Urban Green Volume Using Waveform Airborne Lidar. *Sci. Rep.* **2017**, *7*, 45571. [CrossRef] [PubMed]
49. LARP Larp Unina/PrismaTool. Available online: https://github.com/LarpUnina/PrismaTool (accessed on 31 July 2024).
50. Ghasemi, N.; Justo, J.A.; Celesti, M.; Despoisse, L.; Nieke, J. Onboard Processing of Hyperspectral Imagery: Deep Learning Advancements, Methodologies, Challenges, and Emerging Trends. *arXiv* **2024**, arXiv:2404.06526.
51. Signoroni, A.; Savardi, M.; Baronio, A.; Benini, S. Deep Learning Meets Hyperspectral Image Analysis: A Multidisciplinary Review. *J. Imaging* **2019**, *5*, 52. [CrossRef] [PubMed]
52. Sothe, C.; De Almeida, C.M.; Schimalski, M.B.; La Rosa, L.E.C.; Castro, J.D.B.; Feitosa, R.Q.; Dalponte, M.; Lima, C.L.; Liesenberg, V.; Miyoshi, G.T.; et al. Comparative Performance of Convolutional Neural Network Weighted and Conventional Support Vector Machine and Random Forest for Classifying Tree Species Using Hyperspectral and Photogrammetric Data. *GIScience Remote Sens.* **2020**, *57*, 369–394. [CrossRef]
53. Delogu, G.; Caputi, E.; Perretta, M.; Ripa, M.N.; Boccia, L. Using PRISMA Hyperspectral Data for Land Cover Classification with Artificial Intelligence Support. *Sustain. Switz.* **2023**, *15*, 13786. [CrossRef]
54. Lou, C.; Al-qaness, M.A.A.; AL-Alimi, D.; Dahou, A.; Abd Elaziz, M.; Abualigah, L.; Ewees, A.A. Land Use/Land Cover (LULC) Classification Using Hyperspectral Images: A Review. *Geo-Spat. Inf. Sci.* **2024**, *27*, 1–42. [CrossRef]
55. Ma, L.; Liu, Y.; Zhang, X.; Ye, Y.; Yin, G.; Johnson, B.A. Deep Learning in Remote Sensing Applications: A Meta-Analysis and Review. *ISPRS J. Photogramm. Remote Sens.* **2019**, *152*, 166–177. [CrossRef]
56. Hu, W.; Huang, Y.; Wei, L.; Zhang, F.; Li, H. Deep Convolutional Neural Networks for Hyperspectral Image Classification. *J. Sens.* **2015**, *2015*, 1–12. [CrossRef]
57. Jena, B.; Saxena, S.; Nayak, G.K.; Saba, L.; Sharma, N.; Suri, J.S. Artificial Intelligence-Based Hybrid Deep Learning Models for Image Classification: The First Narrative Review. *Comput. Biol. Med.* **2021**, *137*, 104803. [CrossRef]
58. Congalton, R. Accuracy Assessment and Validation of Remotely Sensed and Other Spatial Information. *Int. J. Wildland Fire* **2001**, *10*, 321–328. [CrossRef]
59. Grandini, M.; Bagli, E.; Visani, G. Metrics for Multi-Class Classification: An Overview. *arXiv* **2020**, arXiv:2008.05756.
60. Naidu, G.; Zuva, T.; Sibanda, E.M. A Review of Evaluation Metrics in Machine Learning Algorithms. In Proceedings of the Artificial Intelligence Application in Networks and Systems; Silhavy, R., Silhavy, P., Eds.; Springer International Publishing: Cham, Switzerland, 2023; pp. 15–25.
61. Li, J. *Satellite Remote Sensing Technologies*; Space Science and Technologies; Springer Singapore: Singapore, 2021; ISBN 9789811548703.
62. Norme per Lo Sviluppo Degli Spazi Verdi Urbani, Italian Republic lawn. 10 of 14/01/2013, GU General Series, n. 27 of 01/02/2013, 13G00031. Available online: https://www.gazzettaufficiale.it/eli/id/2013/02/01/13G00031/sg (accessed on 7 October 2024).
63. Criteri Ambientali Minimi per il Servizio di Gestione del Verde Pubblico e la Fornitura di Prodotti per la Cura del Verde, Italian Republic Ministerial decree n. 63 of 10/03/2020, GU general series, n. 90 of 04/04/2020, 20A01904. Available online: https://www.gazzettaufficiale.it/eli/id/2020/04/04/20A01904/sg (accessed on 7 October 2024).
64. Rossi, L.; Menconi, M.E.; Grohmann, D.; Brunori, A.; Nowak, D.J. Urban Planning Insights from Tree Inventories and Their Regulating Ecosystem Services Assessment. *Sustainability* **2022**, *14*, 1684. [CrossRef]
65. Shaik, R.; Periasamy, S.; Zeng, W. Potential Assessment of PRISMA Hyperspectral Imagery for Remote Sensing Applications. *Remote Sens.* **2023**, *15*, 1378. [CrossRef]